Optica Applicata, Vol. XXXIII, No. 2–3, 2003

Conversion efficiency and the beam-quality factors of the second-harmonic interaction in the molecular crystal (-)2-α-(methylbenzylamino)-5-nitropyridine

PRIMOZ KERKOC

Science and Research Centre of the Republic of Slovenia, Garibaldijeva 18, 6000 Koper, Slovenia,
e-mail: primoz.kerkoc@guest.arnes.si.

The second-harmonic conversion efficiency was calculated for the biaxial molecular crystal (-)2-α-(methylbenzylamino)-5-nitropyridine (MBANP) under high power conditions. The dependence of the second-harmonic efficiency on the beam walk-off angles and the crystal length is discussed. A maximum efficiency of 60% was calculated for the input peak power of 7 kW with a beam radius of 0.15 mm and the interaction length of 1.5 cm. The quality of the second-harmonic and the fundamental beams involved was assessed by the beam-quality factors M^2. For the second -harmonic beam, the beam-quality factors M_y^2 and M_x^2 are 2.6 and 1.4, respectively.

Keywords: nonlinear optics, second-harmonic generation, biaxial crystals.

1. Introduction

Over the past decade there has been observed an intensive development of molecular crystals for applications in nonlinear optics. Many of these π-electron delocalized systems (with donor and acceptor groups) possess optical nonlinearity of the second order similar to, or larger than that of the current inorganic materials. Since the optical quality of these materials is high and they can be prepared with suitable dimensions, one can anticipate their future use in high power applications [1]. In order to use the full potential of the high second-order nonlinear optical susceptibilities of these materials it is advisable to make an analysis of their performance, which includes interactions taking place under high power conditions.

The crystal (-)2-α-(methylbenzylamino)-5-nitropyridine (MBANP) is, at the present time, one of the most extensively investigated molecular crystals [2]. It is monoclinic and therefore exhibits the most general features that can be found in crystals of higher than triclinic symmetry. The biaxial MBANP crystal has two molecules in the unit cell ($Z = 2$) and belongs to space group $P2_1$. The values of the

lattice parameters are a = 0.5409 nm, b = 0.6371 nm, c = 1.7968 nm and β = 94.60°, where the polar crystallographic b-axis is two-fold by symmetry [3]. In MBANP, a substantial "dispersion of the axes" is found between 1064 and 532 nm. The two principal axes of the index ellipsoid (or the principal dielectric axes), which are orthogonal to the monoclinic twofold axis, rotate about the monoclinic axis by about 27° [2]. For frequency doubling two different principal dielectric systems exist, which complicates the analysis and introduces new significant features.

Here, the analysis simulates frequency doubling with a 1064 nm fundamental, which is often carried out for the evaluation of nonlinear optical properties of the second order. A Fourier transform method was applied in order to solve the system of partial differential equations describing the coupling between the second-harmonic and fundamental electric fields in the crystal, including the effects of beam walk-off, depletion, optical absorption and diffraction. Asymmetric diffraction of light in the birefringent medium was ignored since it is a correction of the second order [4]. The conversion efficiency of second-harmonic generation was calculated as a function of the input energy of a pulse with the length of 15 ns, the beam-walk angles and the interaction length. The quality of the fundamental and generated beams was quantified by use of the M^2 factors.

2. Beam walk-off angles

To calculate the beam walk-off angles of MBANP, the three principal values of the refractive index and the orientation of the dielectric axes at both frequencies were taken from [2] and the directions **s**, for type I phase-matching, were calculated (Tab. 1). Then the Poynting vectors $\mathbf{t}^{\Omega}(\Omega = 2\omega, \omega)$ in the principal dielectric systems were determined using relations found in [5] (for details, see [6]). After a linear transformation their components were obtained in the standard orthogonal piezoelectric system (a^*, b, c) where b and c are the lattice vectors and a^* is the reciprocal lattice vector normal to the (b, c) plane. The beam walk-off angles ρ^{Ω}, defined as angles between phase-matching direction **s** and the Poynting vectors $\mathbf{t}^{\Omega}$, were then calculated from equation

$$\cos\rho^{\Omega} = \mathbf{t}^{\Omega} \cdot \mathbf{s}. \tag{1}$$

An orthogonal phase-matching system $x \| \mathbf{D}^{\omega}$, $y \| \mathbf{D}'^{2\omega}$ and $z \| \mathbf{s}$ was defined, where $\mathbf{D}^{\omega}$ is the dielectric displacement vector of the fundamental wave. The vector $\mathbf{D}'^{2\omega}$ is

T a b l e 1. Principal values of the refractive indices and the relative orientation of the indictrix in the orthogonal system (a^*, b, c) for both wavelengths used in this calculation (see [2]). The angle $\Phi_{\Omega}(\Omega = 2\omega, \omega)$ is the rotation about the positive b-axis needed to bring the a^*-axis into the coincidence with the x'-axis.

λ [nm]	$n_{x'}$	$n_{y'}$	$n_{z'}$	Φ_{Ω} [°]
1064	1.6550	1.7144	1.6882	–14.0
532	1.6895	1.8584	1.7632	13.0

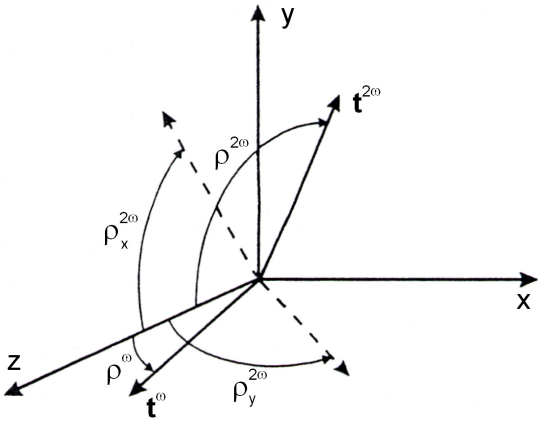

Fig. 1. Orthogonal phase-matching system $x||\mathbf{D}^{\omega}$, $y||\mathbf{D}'^{2\omega}$ and $z||\mathbf{s}$ of the MBANP molecular crystal. The propagation of the waves at both frequencies is in the z-direction. The angle ρ^{ω} is the beam walk-off of the fundamental beam with the Poynting vector $\mathbf{t}^{\omega}$ propagating in the (x, z) plane. Direction of the second -harmonic Poynting vector is denoted by $\mathbf{t}^{2\omega}$ and its beam walk-off angle by $\rho^{2\omega}$. The projections of this angle onto (y, z) and (x, z) are denoted by $\rho_x^{2\omega}$ and $\rho_y^{2\omega}$, respectively. For clarity, the angles are shown in enormous proportions.

T a b l e 2. Values of the parameters of MBANP crystals used in the computation. The quantity d_{eff} is the effective nonlinear susceptibility of the second-order, the angles ρ^{ω} and $\rho^{2\omega}$ are beam walk-off angles of the fundamental and second-harmonic waves. The angles $\rho_x^{2\omega}$ and $\rho_y^{2\omega}$ are projections of the angle $\rho^{2\omega}$, as defined in Fig. 1. The absorption coefficients are $\alpha_{2\omega}$ and α_{ω} and n is the refractive index of the phase-matching [6].

d_{eff} [pm/V]	ρ^{ω} [°]	$\rho^{2\omega}$ [°]	$\rho_x^{2\omega}$ [°]	$\rho_y^{2\omega}$ [°]	$\alpha_{2\omega}$ [cm^{-1}]	α_{ω} [cm^{-1}]	n
6.5	0.51	2.29	2.27	0.31	0.045	0.038	1.700

the component of the second-harmonic displacement perpendicular to the (x, z) plane and $\mathbf{s}$ is the unit vector of the phase-matching direction. Since propagation is not in a dielectric plane, fixed for both frequencies, vectors $\mathbf{D}^{\omega}$ and $\mathbf{D}^{2\omega}$ are not orthogonal. Consequently, $\mathbf{t}^{2\omega}$ lies in neither the (x, z) nor the (y, z) plane, which presents additional difficulty in further analysis (see Fig. 1). For this reason the beam walk-off angle of the second-harmonic wave $\rho^{2\omega}$ was projected onto the (x, z) and (y, z) planes as:

$$\cos\rho_x^{2\omega} = \frac{\cos\rho^{2\omega}}{\sin\delta_x} \tag{2a}$$

$$\cos\rho_y^{2\omega} = \frac{\cos\rho^{2\omega}}{\sin\delta_y} \tag{2b}$$

where δ_x and δ_y are the angles between the second-harmonic Poynting vector $\mathbf{t}^{2\omega}$, and vectors $\mathbf{D}^{\omega}$ and $\mathbf{D}^{2\omega}$, respectively. The values of the beam-walk angles are given in Tab. 2.

3. Second-harmonic generation

The simulation assumes that the crystal is unbounded in the transverse directions. The amplitudes of the electric fields decrease to zero with an increase in radial distance from the phase-matching direction and are negligible on the lateral boundaries of the crystal. For normal incidence, the equations for the amplitude of the fundamental wave A_ω and the second-harmonic waves $A_{2\omega}$ in the depleted and slowly varying amplitude formulations are [7]:

$$\frac{\partial A_\omega}{\partial z} + \frac{\alpha_\omega}{2} A_\omega + \rho^\omega \frac{\partial A_\omega}{\partial x} - \frac{1}{2ik_\omega}\left(\frac{\partial^2 A_\omega}{\partial x^2} + \frac{\partial^2 A_\omega}{\partial y^2}\right) = -i \frac{\omega d_{\text{eff}}}{c n_\omega} A_{2\omega} A_\omega^* \exp(-i\Delta k z), \tag{3a}$$

and

$$\frac{\partial A_{2\omega}}{\partial z} + \frac{\alpha_{2\omega}}{2} A_{2\omega} + \rho_y^{2\omega} \frac{\partial A_{2\omega}}{\partial x} + \rho_x^{2\omega} \frac{\partial A_{2\omega}}{\partial y} - \frac{1}{2ik_{2\omega}}\left(\frac{\partial^2 A_{2\omega}}{\partial x^2} + \frac{\partial^2 A_{2\omega}}{\partial y^2}\right) = -i \frac{\omega d_{\text{eff}}}{c n_{2\omega}} A_\omega^2 \exp(i\Delta k z). \tag{3b}$$

We have two coupled second-order nonlinear partial differential equations describing the propagation of the electric fields through the crystal. This formulation includes diffraction effects and terms in and accounting for optical absorption. The terms involving ρ^ω, ρ_x^ω and ρ_y^ω describe the effect of beam walk-off. The wave vectors at the fundamental frequency ω and second-harmonic frequency 2ω are k_ω and $k_{2\omega}$, respectively, d_{eff} is the effective nonlinear optical susceptibility, c is the speed of light in vacuum, $n_{2\omega}$ and n_ω are the refractive indices of the second-harmonic and fundamental waves, respectively. The phase-mismatch is denoted by Δk. In order to account for the intensity-dependent phase shifts of second-harmonic and fundamental pulses, the electric field amplitudes are time dependent, that is $A(x, y, z, t)$ [8].

Applying Fourier transform, $B(p, q, z, t) = F(A(x, y, z, t))$, to Eqs. (3) and using the elementary rules for the Fourier transformation of derivatives, one obtains the following equations:

$$\frac{\partial B_\omega}{\partial z} + \frac{\alpha_\omega}{2} B_\omega - i\left[2\pi\rho^\omega p + \frac{2\pi^2}{k_\omega}(p^2 + q^2)\right] B_\omega = -i \frac{\omega d_{\text{eff}}}{c n_\omega} \exp(-i\Delta k z) F(A_{2\omega} A_\omega^*), \tag{4a}$$

$$\frac{\partial B_{2\omega}}{\partial z} + \frac{\alpha_{2\omega}}{2} B_{2\omega} - i\left[2\pi(\rho_y^{2\omega} p + \rho_x^{2\omega} q) + \frac{2\pi^2}{k_{2\omega}}(p^2 + q^2)\right] B_{2\omega}$$

$$= -i \frac{\omega d_{\text{eff}}}{c n_{2\omega}} \exp(i\Delta k z) F(A_\omega^2). \tag{4b}$$

The TEM_{00} mode of the Gaussian spatial and temporal dependences was inserted at the input surface ($z = 0$) and sliced in time by the interval Δt. Only Fresnel loss at this surface was taken into account since nonlinear optical reflection can be neglected. This is justifiable for propagation directions of light into or close to the phase-matching direction where the amplitude of the second-harmonic wave can be neglected at the input surface.

For each time slice, at the beginning of each step z, the corresponding products of the electric fields on the right-hand side of Eqs. (3) were calculated, Fourier transformed by the FFT algorithm and inserted into Eqs. (4), see [8], [9]. To yield the Fourier transforms of the electric field, at $z + \Delta z$, the integration over each step was carried out by the semi-implicit extrapolation method with an adaptive step size control [10]. Before integration the substitution, as suggested in [4], was applied in order to eliminate the diffraction and the beam walk-off terms from the left-hand side of Eqs. (4). It was pointed out that this makes the computation more efficient [4]. After applying the inverse substitution, the solutions were transformed by the inverse Fourier transform to calculate the amplitudes of the electric fields at a distance $z + \Delta z$. The procedure was repeated over the whole crystal length. At the end, both pulses (second -harmonic and fundamental) were composed from the time slices calculated as described above. After the interaction length z, the resulting electric field distribution of the second-harmonic wave was multiplied by its complex conjugate and the energy of the second-harmonic pulse was obtained by numerical integration of the intensity over the two space variables, x and y, and the time t.

4. Beam-quality factors

The beam quality can be assessed by use of the beam-quality factors M^2. For a purely Gaussian ideal distribution the value of factor M^2 is one, but real beams have M^2 larger than one. The values of factors M^2 have been calculated for the second-harmonic and fundamental beams by the theory outlined in [11], [12]. The transverse moments of the optical pulse are based on the intensity integrated over the time dependence of the pulse (fluence). The calculation begins by defining the quantity U as:

$$U = \int_{-\infty}^{\infty} \int_{-\infty}^{\infty} \int_{-\infty}^{\infty} |A(x, y, t)|^2 \, \mathrm{d}x \, \mathrm{d}y \, \mathrm{d}t, \tag{5a}$$

$$U = \int_{-\infty}^{\infty}\int_{-\infty}^{\infty}\int_{-\infty}^{\infty} |B(p, q, t)|^2 \mathrm{d}p\mathrm{d}q\mathrm{d}t. \tag{5b}$$

The first moments are defined as

$$\bar{x}(z) = \frac{1}{U}\int_{-\infty}^{\infty}\int_{-\infty}^{\infty}\int_{-\infty}^{\infty} x|A(x, y, z, t)|^2 \mathrm{d}t\mathrm{d}x\mathrm{d}y, \tag{6a}$$

$$\bar{p} = \frac{1}{U}\int_{-\infty}^{\infty}\int_{-\infty}^{\infty}\int_{-\infty}^{\infty} p|B(p, q, t)|^2 \mathrm{d}t\mathrm{d}p\mathrm{d}q. \tag{6b}$$

The first spatial moment propagates as [11]:

$$\bar{x}(z) = \bar{x}(0) + \lambda z\bar{p}. \tag{7}$$

The fluence based variances of the beam shape are given by:

$$\sigma_x^2(z) = \frac{1}{U}\int_{-\infty}^{\infty}\int_{-\infty}^{\infty} [x - \bar{x}(z)]^2 \left[\int_{-\infty}^{\infty} |A(x, y, z, t)|^2 \mathrm{d}t\right] \mathrm{d}x\mathrm{d}y, \tag{8a}$$

$$\sigma_p^2 = \frac{1}{U}\int_{-\infty}^{\infty}\int_{-\infty}^{\infty} [p - \bar{p}(z)]^2 \left[\int_{-\infty}^{\infty} |B(p, q, t)|^2 \mathrm{d}t\right] \mathrm{d}p\mathrm{d}q. \tag{8b}$$

The beam variance $\sigma_x^2(z)$ in the transversal x-direction propagates as

$$\sigma_x^2(z) = \sigma_x^2(0) - [A_x(0) + 2\lambda\bar{x}(0)\bar{p}]z + \lambda^2\sigma_p^2 z^2$$

where

$$A_x(z) = \frac{\lambda}{\pi U}\int_{-\infty}^{\infty}\int_{-\infty}^{\infty} x\left\{\int_{-\infty}^{\infty} \mathrm{d}t\,\mathrm{Im}\left[A(x, y, z, t)\,\frac{\partial}{\partial x}A^*(x, y, z, t)\right]\right\}\mathrm{d}x\mathrm{d}y. \tag{9}$$

The formulas for the minimum variance of the beam shape or the beam waist $\sigma_{0x}^2(z)$ and for the beam-quality factor M_x^2 in the transversal x-direction then become

$$\sigma_{0x}^2 = \sigma_x^2(z) - \frac{[A_x(z) + 2\lambda\bar{x}(z)\bar{p}]^2}{4\lambda^2\sigma_p^2}, \tag{10}$$

$$M_x^2 = 4\pi\sigma_{0x}^2\sigma_p^2. \tag{11}$$

The beam-quality factor M_x^2 characterises the beam quality when projected onto the (x, z) phase-matching plane (see Fig. 1). Similar expressions exist for the value of M_y^2, *i.e.*, the beam quality factor characterising the projection of the beam shape onto the phase-matching (y, z) plane.

The calculations were performed for the phase-matching direction (Δk = 0) corresponding to the largest effective nonlinear optical coefficient of MBANP (d_{eff} = 6.5 pm/V) [6]. This phase-matching direction is at the angle ϕ = 121.1° and θ = 51.2° from the a* and b axes, respectively. The optical absorption coefficients in this direction were calculated from the data and the procedure given in [13]. The input peak power follows from the radius at the input face and the input peak intensity. The third parameter defining the Gaussian input beam is the position of its focus before increasing the input power to a level at which depletion becomes significant. The analysis at a beam radius of 0.1 mm has shown that shifting the focal position over the whole crystal length makes only a 1% difference in the efficiencies. At a beam radius of 0.15 mm and above this difference is negligible. Therefore, for the range of parameters used in the calculations, the position of the focus is irrelevant. A value of 20 MW/cm^2 was chosen for the intensity since it is near the optical damage threshold observed in the second-harmonic generation experiments. The dependence of the second-harmonic conversion efficiency on the interaction length is presented in

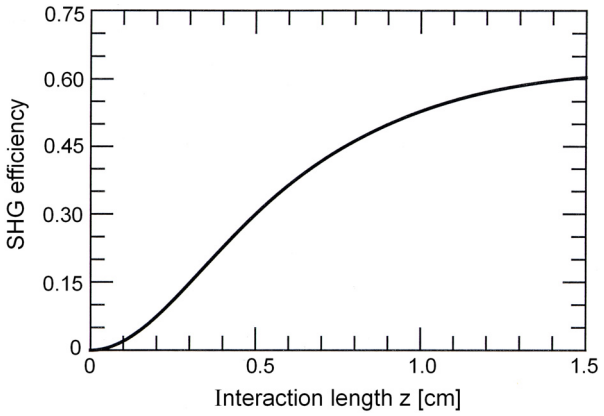

Fig. 2. Dependence of the second-harmonic efficiency on the interaction length for MBANP. The value of input peak power of the fundamental beam is 7 kW (pulse length 15 ns). The input peak intensity has a value of 20 MW/cm^2.

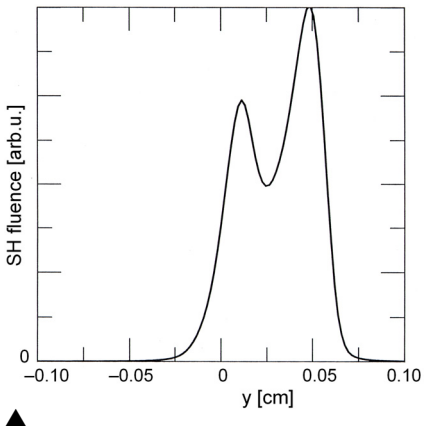

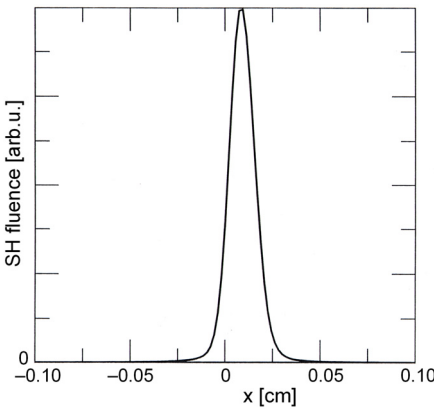

▲

Fig. 3. Projection of the second-harmonic beam onto the (y, z) plane of the phase-matching system.

Fig. 4. Projection of the second-harmonic beam onto the (x, z) plane of the phase-matching system.

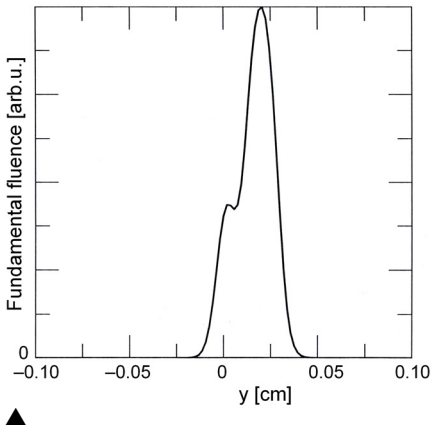

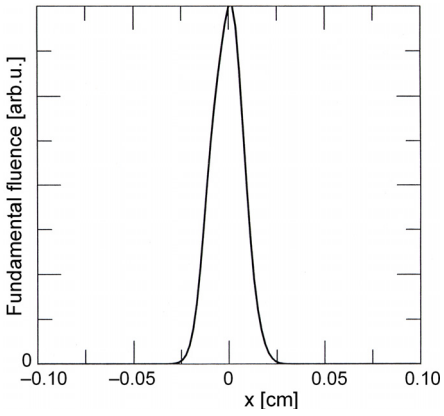

▲

Fig. 5. Projection of the fundamental beam onto the (y, z) plane of the phase-matching system.

Fig. 6. Projection of the fundamental beam onto the (x, z) plane of the phase-matching system.

Fig. 2. It was found that a beam with the input peak power of 7 kW and the radius of 0.15 mm produces the maximum efficiency of 60% in MBANP (the pulse length of 15 ns, the interaction length of 1.5 cm). Using the calculated electric fields, the beam -quality factors M^2 for the fundamental and second-harmonic beams were determined from Eqs. (5)–(11). For the second-harmonic beam, the calculated beam-quality factors M_x^2 and M_y^2 are 2.6 and 1.4, respectively. The corresponding beam-quality factors of the fundamental beam are 2.0 and 1.3, respectively. The projections of the beam shapes onto the (x, z) and (y, z) planes of the phase-matching system are shown in Figs. 3–6.

5. Conclusion

This work presents a solution of the system of partial differential equations describing the coupling between the electric fields produced in the second-harmonic generation. The equations were solved systematically by use of a two-dimensional Fourier transform. The simulation was extended to the characteristic biaxial features of MBANP, taking account of the rotation with frequency (angular dispersion) of dielectric axes and the consequent more complicated relationship between the Poynting vectors at the two frequencies. To account for these biaxial features, it was also necessary to modify the theory for the calculation of the beam-quality factors.

Acknowledgments – This work was supported in part by the Ministry of the Education, Science and Sport of the Republic of Slovenia.

References

[1] BAILEY R.T., CRUICKSHANK F.R., PUGH D., SHERWOOD J.N., Acta Crystallogr. A **47** (1991), 145.
[2] BAILEY R.T., CRUICKSHANK F.R., PUGH D., SHERWOOD J.N., SIMPSON G.S., WILKIE S., Mol. Cryst. Liq. Cryst. **231** (1993), 223.
[3] TWIEG R.J., DIRK C.W., Research Report RJ 5237 (54077), 1968, IBM Almaden Research Center San Jose, CA.
[4] ARISHOLM G.J., Opt. Soc. Am. B **14** (1997), 2543.
[5] BORN M., WOLF E., *Principles of Optics*, Pergamon, Oxford 1980, pp. 665-678.
[6] KERKOC P., BAILEY R.T., CRUICKSHANK R.F., PUGH D., J. Opt. Soc. Am. B **15** (1998), 438.
[7] AKHMANOV S.A., KOVRYGIN A.I., SUKHORUKOV A.P., *Quantum Electronics: A Treatise*, Part B, [Eds.] H. Rabin and C.L. Tang, Academic, New York 1975, p. 511.
[8] SMITH A.V., BOWERS M.S., J. Opt. Soc. Am. B **12** (1995), 49.
[9] PRESS W.H., FLANNERY B.P., TEUKOLSKY S.A., VETTERLING W.T., *Numerical Recipes in FORTRAN 77: The Art of Scientific Computing*, University Press, Cambridge 1992, pp. 515–519.
[10] *Ibidem*, pp. 735–519.
[11] SMITH A.V., ALFORD W.J., RAYMOND T.D., BOWERS M.S., J. Opt. Soc. Am. B **12** (1995), 2253.
[12] SIGMAN A.E., IEEE J. Quantum Electron. **27** (1993), 1146.
[13] KERKOC P., BAILEY R.T., CRUICKSHANK R.F., PUGH D., SHERWOOD J.N., Opt. Commun. **132** (1996), 484.

Received September 19, 2002
in revised form October 28, 2002